Title
MECHANICAL PROPERTIES AND FRACTURE BEHAVIOR OF CHEMICALLY BONDED COMPOSITES

Author
Stett, Mark Alexander.

Publication Date
1969-04-01

UCRL-18762

eq. 2

MECHANICAL PROPERTIES AND FRACTURE BEHAVIOR OF CHEMICALLY BONDED COMPOSITES

Mark Alexander Stett
(Ph. D. Thesis)

April 1969

AEC Contract No. W-7405-eng-48

LAWRENCE RADIATION LABORATORY
UNIVERSITY of CALIFORNIA BERKELEY

UCRL-18762

eq. 2

DISCLAIMER

TABLE OF CONTENTS

MECHANICAL PROPERTIES AND FRACTURE BEHAVIOR OF CHEMICALLY BONDED COMPOSITES

Mark Alexander Stett

Inorganic Materials Research Division, Lawrence Radiation Laboratory,
and Department of Materials Science and Engineering,
College of Engineering, University of California,
Berkeley, California

ABSTRACT

April 1969

The effect of chemical bonding between phases of a glass-metal composite on the strength and fracture behavior was investigated. When no chemical bonding occurs, strengthening can be achieved through the mechanical formation of an interface between dispersant and matrix. By the formation of a chemical bond, an even greater strengthening can be obtained. Strengthening occurs by the limitation of the Griffith flaw size and is controlled by micromechanical stress concentrations developed upon loading. Internal stresses developed upon cooling from the fabrication temperature control the path of fracture. The existence of a chemical bond serves to counteract the micromechanical stress concentration and therefore increase the strength.

I. INTRODUCTION

Many of today's new materials are multiphase or composite in nature. Dispersion strengthened alloys make use of a finely divided second phase distributed in a crystalline matrix. Glass-ceramics make use of controlled crystallization from a glassy melt. Fiber reinforced resins have been used extensively in the area of organic materials. The properties of composite materials will depend upon the properties of the individual components, their distribution, and their physical and chemical interaction.

In developing an understanding of the properties of brittle-matrix composites, the obvious choice for the matrix is glass--the ideal brittle material. Fulrath[1] demonstrated that by vacuum hot pressing, a continuous matrix of glass containing a dispersed phase could be fabricated. Since that time extensive studies on the elastic and mechanical properties of such systems have been reported.[2-13] In all the previous studies the interfacial bonding characteristics between the dispersion and the matrix have not been clearly identified.

Nason[3] first encountered the problem of interfacial bonding in attempting to disperse tungsten and nickel microspheres in glass matrices where the matrix thermal expansion coefficient was selected to be either less than or greater than that of the dispersed material. When the thermal expansion coefficient of the glass was less than that of the nickel metal and there was no bonding between phases, the nickel shrank away from the glass upon cooling and formed pseudoporosity. Composites fabricated by Nason from tungsten and a glass of lower thermal expansion coefficient, however, showed an anomalous strengthening. He then hot

pressed under the same conditions some of this glass against a well-polished disc of tungsten. Adherence was observed between the tungsten and glass. A similar experiment using a nickel disc and another glass with a lower thermal expansion coefficient than that of nickel showed no adherence.

Bertolotti and Fulrath[10] used this thermal expansion mismatch and lack of interfacial bonding in order to create a controlled amount of spherical porosity of known size in their examination of porous glass. With small particle sizes, they also observed an anomalous strengthening and proposed that adsorbed water on the surface of the glass powder used in fabricating the composite caused a slight oxidation of the nickel surface and resulted in a bond between the oxidized nickel and the glass. As a result of this observation, a more extensive study of the effect of a chemical bond between phases in a brittle matrix composite was undertaken.

II. THEORY

In attempting to analyze this system, we must consider two types of stresses. Internal stresses are created between glassy and crystalline phases during cooling as a result of the difference in the thermal expansions of the two phases. Under mechanical loading, differences in the elastic properties of individual components can lead to localized concentration of the applied stress. The existence of a bond further complicates the situation.

A. Internal Stresses

As a result of differences in thermal expansion among phases in a polycomponent material, internal stresses are developed upon cooling from the fabrication temperature. It has often been proposed that internal stresses affect the mechanical strength of composite materials.

A means of calculating this internal stress was provided by Selsing[14] and shown to be accurate for a crystalline material of high modulus of elasticity embedded in a glass of low modulus of elasticity:

$$P_r = -2P_t = \frac{\Delta\alpha\Delta T}{\frac{1+\mu_G}{2E_G} + \frac{1-2\mu_M}{E_M}} \quad \frac{R^3}{r^3} \qquad (1)$$

where P_r = radial internal stress

P_t = tangential internal stress

$\Delta\alpha$ = difference in thermal expansion

E_G = Young's modulus of the glass

E_M = Young's modulus of the metal dispersed phase

ΔT = temperature differential

μ_G = Poisson's ratio of the glass

μ_M = Poisson's ratio of the metal dispersed phase

R = Particle radius

r = radius under consideration

Without a detailed knowledge of the viscous behavior of the glass being used, however, it is difficult to estimate what value should be used for ΔT. The difference between the test temperature and the temperature at which the viscosity of the glass is high enough to support stress should be used.

Fulrath[1] has shown that internal stresses could be detected in ceramic bodies by X-ray diffraction techniques. After correction for beam penetration and camera geometry, peak shifts give an accurate measurement of strain. An increase in peak angle is indicative of compression while a decrease in peak angle corresponds to tension. A more detailed analysis of the technique and examples of its application were presented by Grossman and Fulrath.[15]

B. Applied Stresses

Theoretical solutions exist for stress concentrations associated with elastic inhomogeneities of various shapes in an infinite matrix under load. Since glass fracture is usually nucleated at the specimen surface and because of the high stress gradients away from the surface in the strength test, Goodier's solutions for a circular inclusion in a flat plate were used.[16]

For a circular hole in a plate it is found that the expression for the tangential stress concentration yields tensile stresses greater than the applied stress under conditions of tensile load. The expression

for this stress concentration is

$$\sigma_t = 2T\left[\frac{R^2}{4r^2} - \frac{3R^4}{4r^4}\cos 2\theta\right] + T \sin \theta \qquad (2)$$

where T = applied tensile load

θ = angle from direction of applied tension = 90° for maximum stress concentration in this case

R = hole radius

r = radius under consideration

For a simple tension, T, in one direction there is a maximum stress concentration of 3T at the hole as can be seen in Fig. 1. This stress concentration decreases rapidly to only 1.2T at a distance of R into the matrix. The stress concentration also decreases rapidly as θ moves away from 90°, confining the stress concentration to small regions at A and B.

In the case of a rigid inclusion, contact with the surrounding material produces a different type of stress concentration. A rigid inclusion in simple tension induces a tension at C and D which can be as much as 1.5T. The expression for this stress concentration is:

$$\sigma_r = 2G_G\left[-\frac{A}{r^2} + \left(\frac{3B}{r^4} - \frac{2C}{r^2}\right)\cos 2\theta\right] + \frac{T}{2}(1 + \cos 2\theta) \qquad (3)$$

where

$$A = \frac{TR^2}{4G_G}\,\frac{(1-2\mu_M)\,G_G - (1-2\mu_G)\,G_M}{(1-2\mu)\,G_G + G_M} \qquad (4)$$

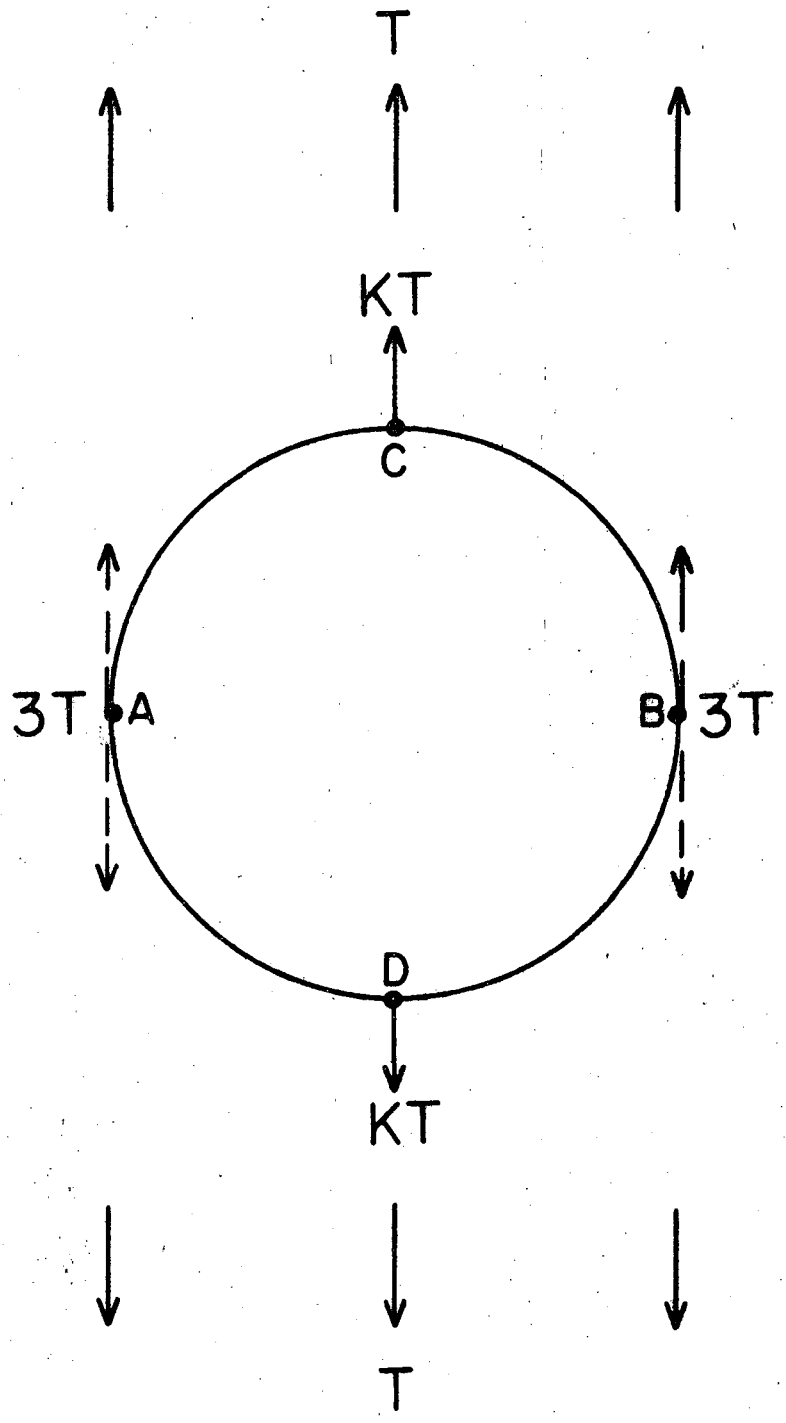

Fig. 1. Stress concentrations developed under an applied tensile load (----- = porosity, _____ = inclusion).

$$B = \frac{TR^4}{4G_G} \frac{G_G - G_M}{G_G + (3-4\mu_G)G_M} \tag{5}$$

$$C = \frac{TR^2}{2G_G} \frac{G_G - G_M}{G_G + (3-4\mu_G)G_M} \tag{6}$$

In these expressions

θ = 0° for maximum stress concentration

G_G = bulk modulus of the glass

G_M = bulk modulus of the metal dispersed phase

and the other terms have been previously defined. The tension at A and B is reduced and becomes compression if μ_G is less than 0.25. The tensile stress concentration at C and D also decreases with increasing R, but less rapidly. A stress concentration of 1.08T is reached at a distance of 4R. The stress concentration once again decreases from a maximum with a change in θ from θ = 0°, confining the stress concentration to regions at C and D.

C. Bonding

A bond is obtained between a glass and a metal when the glass is saturated with the oxide of the metal at the glass-metal interface. According to Pask and Fulrath[17] a chemical bond can occur when a balance of bond energies is achieved across the transition zone at the interface between the glass and the metal. This balance occurs when "thermodynamic equilibrium" is obtained at the interface. By "thermodynamic equilibrium" it is meant that each of the phases is saturated with the lower oxide and

that there is no possibility of further reaction to form a new phase. If the available oxide is entirely dissolved by the glass before the glass attains the saturation concentration, the resultant contact with a purely metallic surface results in a weak bond.

Consider a system composed of nickel and a glass with a lower thermal expansion. In this case the metal will shrink away from the glass upon cooling from the fabrication temperature when there is no pre-oxidation of the nickel and interfacial bond formation. The result will be a glass-pore system and the strength of the composite will be lowered as a result of the introduction of the nickel. This can be seen schematically in Fig. 2a. If the glass comes in contact with pre-oxidized nickel while molten, diffusion of the oxide into the glass occurs. The glass at the oxide interface becomes saturated with the oxide (assuming sufficient oxide is present). This saturation would result in a balance of bond energies and the formation of a chemical bond. Ideally, this balance would occur without a bulk oxide layer at the nickel surface (Fig. 2b). If there is an excess of pre-oxidation, a definite oxide layer will exist between the nickel and the saturated glass (Fig. 2c) and the strength of the resultant composite would reflect the complex interactions between the metal, the oxide layer, and the glass.

D. Strengthening by Flaw Limitation

Hasselman and Fulrath[7] have hypothesized that a dispersion of a hard second phase within a brittle glass matrix will strengthen the composite by limiting the size of Griffith flaws. When the average distance between second phase particles is less than the flaw size, the flaw size is limited to this average mean free path. For a flat plate containing

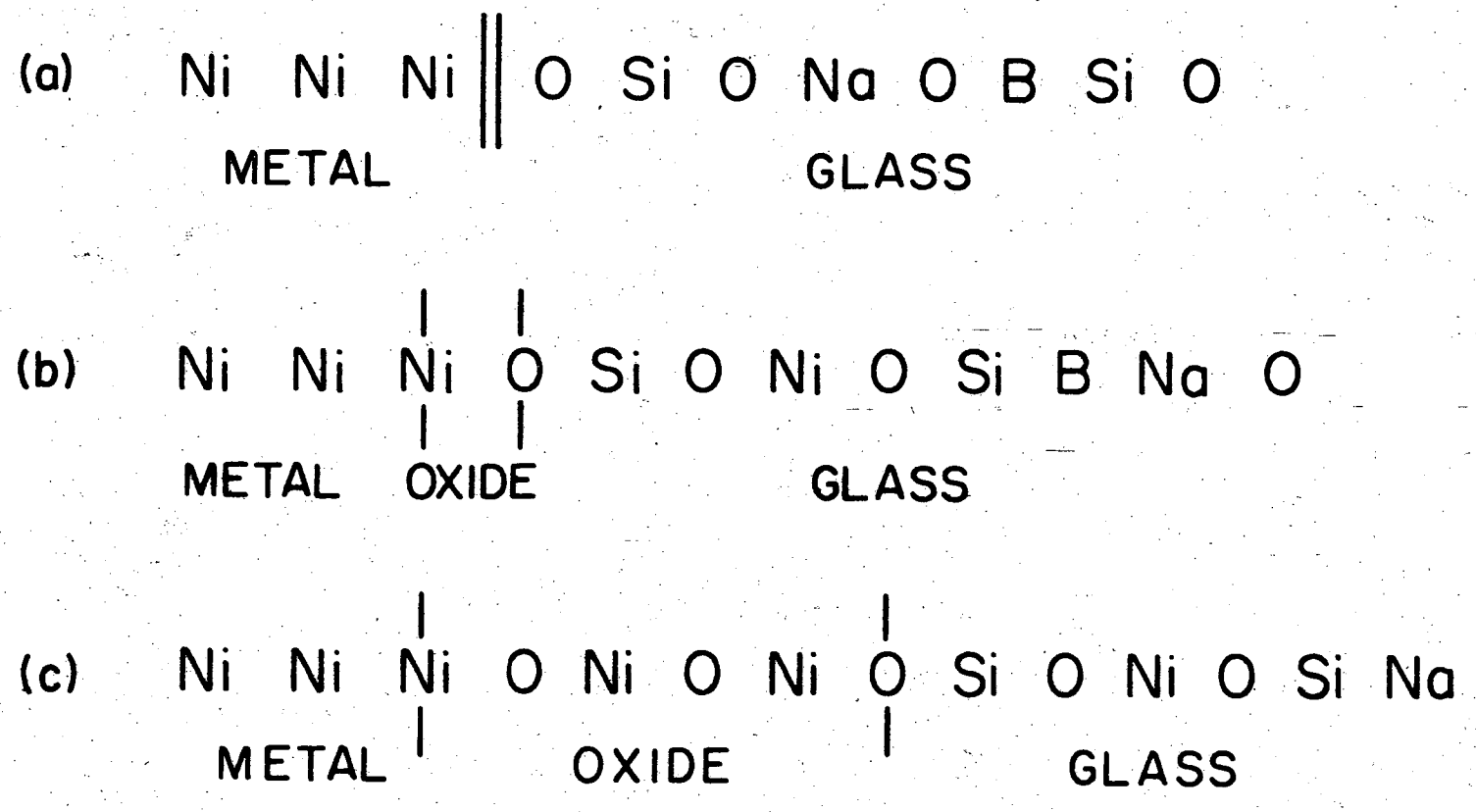

Fig. 2. Schematic diagram of the bonding possibilities between metal and glass.

an elliptical flaw, the Griffith expression for the macroscopic strength, S_o, is

$$S_o = \left(\frac{4\gamma E}{\pi a}\right)^{1/2} \tag{7}$$

where γ is the surface energy, E is Young's modulus of elasticity, and "a" is the flaw size. An expression for the mean free path, d, between spherical particles of uniform radius, R, distributed statistically throughout a matrix was provided by Fullman[18] as

$$d = \frac{4R\,(1-\phi)}{3\phi} \tag{8}$$

where ϕ is the volume fraction of dispersed particles. Substituting Eq. (8) into Eq. (7) we find the strength of a composite that is being strengthened by a flaw limitation mechanism to be

$$S_o = \left(\frac{3\gamma E\phi}{\pi R(1-\phi)}\right)^{1/2} \tag{9}$$

When a given load is applied to the composite there will be, due to the stress concentrations resulting from differences in elastic properties of the phases,[9] areas of higher stress than the applied load. The measured strength will therefore be

$$S_m = \frac{1}{K} S_o \tag{10}$$

By substituting Eq. (10) into Eq. (9) and rearranging this to isolate the variable, $(1/d)^{1/2}$, we find

$$S_m = \left(\frac{4\gamma E}{\pi K}\right)^{1/2} \left(\frac{3\phi}{4R(1-\phi)}\right)^{1/2} \qquad (11)$$

This function was plotted by first calculating the slope from approximate values of K (1.4), γ (10,000 ergs/cm^2), and E (10^7 psi). The assumption of 10,000 ergs/cm^2 for the surface energy is reasonable from two standpoints. It falls within the very wide range of values previously assumed or measured in other investigations and it produces results that are in good agreement with the observed data in this investigation. This value of the surface energy is, however, an assumption and more confidence could be expressed as to its accuracy only if a more detailed study of the fracture surface energy were available. From Eq. (11) it can be seen that this function will necessarily go through the origin. The location of the horizontal portion of the curve was accomplished by determining the strength of each glass alone. At large values of "d" the average mean free path will be larger than the Griffith flaw size and no strengthening will be observed. The horizontal extension of the individual glass strength value will intersect the plotted slope at the size of the Griffith flaw. This behavior can be seen in Fig. 3. In order to assure strengthening in the composites studied here, a combination of particle size and volume fraction was chosen in each case that provided an average mean free path less than the Griffith flaw size.

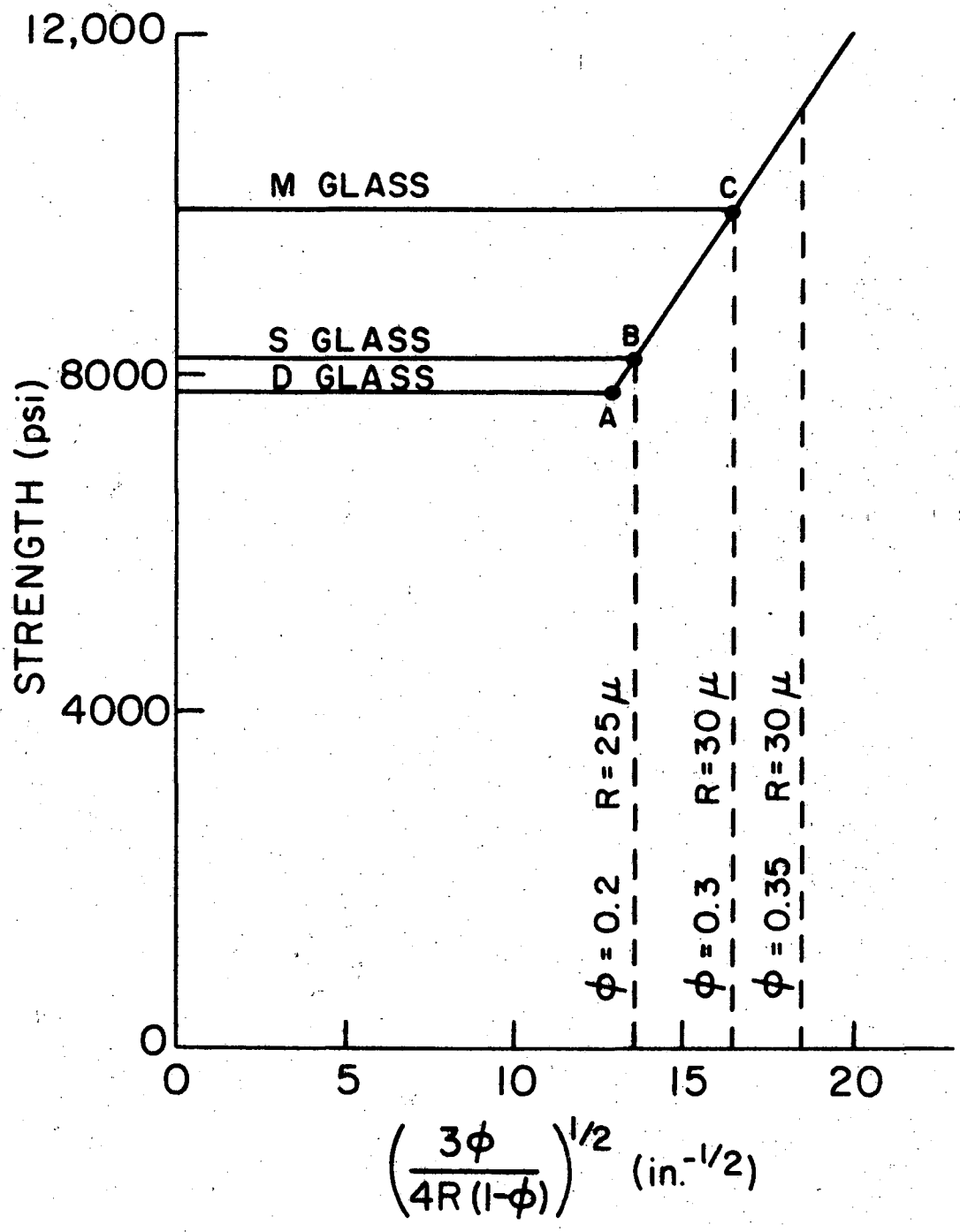

Fig. 3. Calculated composite strength as a function of reciprocal square root of the average mean free path.

III. EXPERIMENTAL PROCEDURE

The glasses used in this investigation were made in the laboratory from silica flour, reagent grade sodium carbonate and boric acid, and alumina. The materials were dry mixed and then melted and refined in a platinum crucible at 1400°C in an electric furnace. Densities of the cast glass were measured using an Archimedes technique with methyl alcohol. The cast glass was crushed and dry ground to -325 mesh in an alumina-lined ball mill with alumina pebbles. Elastic properties of the glasses were measured by the resonance technique of Spinner and Tefft[19] and Pickett.[20] With this method, two values for Young's modulus were obtained for each specimen by calculations using Hasselman's[21] tables. The shear moduli were calculated from an expression of the pertinent shape factor given by Spinner and Tefft.[19] A summary of material properties is given in Table I.

Nickel microspheres were purchased and partitioned by screening into various size fractions in order to obtain desired average particle sizes. In order to evaluate the various oxidation treatments, weight gain tests were carried out at three temperatures. The curves that were obtained were predominantly linear in the ranges that were used and can be seen in Fig. 4. From these data, oxide layer thicknesses and average particle density were calculated and are given in Figs. 5-6. These densities were used along with the measured glass densities to calculate composite batch weights. Scanning electron micrographs of both oxidized and unoxidized spheres are shown in Fig. 7.

The composites were prepared from thoroughly mixed combinations of oxidized nickel spheres and powdered glass and were vacuum hot pressed

Table I

Material Properties

Material	Composition	in/in °C x 10^6 α	psi x 10^{-6} E	μ	gm/cc ρ
Ni		13.9	30.0	0.42	8.9
D glass	70 SiO_2 14 B_2O_3 16 Na_2O	7.7	11.7	0.2	2.47
S glass	55 SiO_2 15 Al_2O_3 30 Na_2O	13.8	9.8	0.2	2.47
M glass	50 SiO_2 13 Al_2O_3 37 Na_2O	16.0	10.2	0.2	2.51

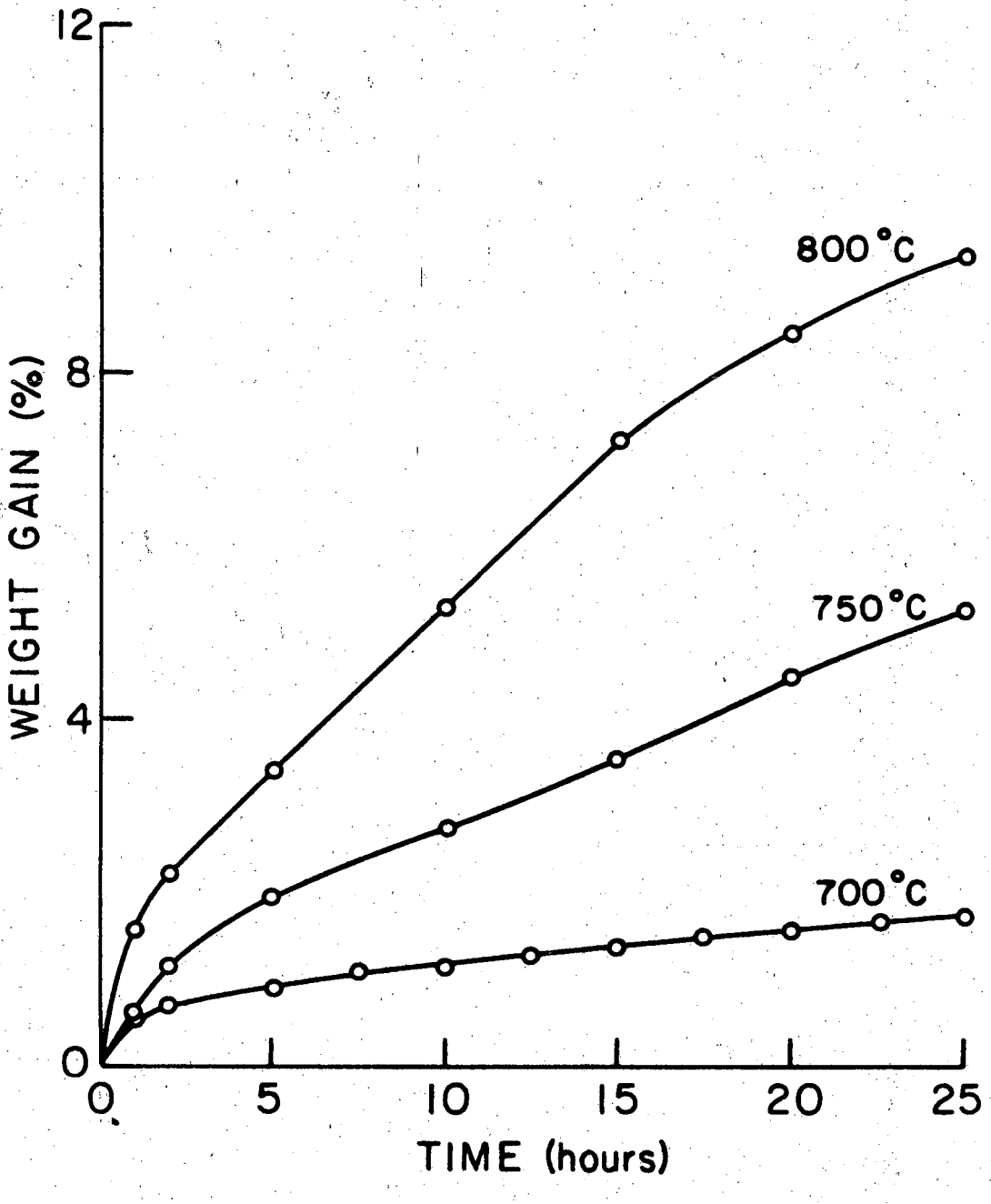

Fig. 4. Oxidation of nickel spheres.

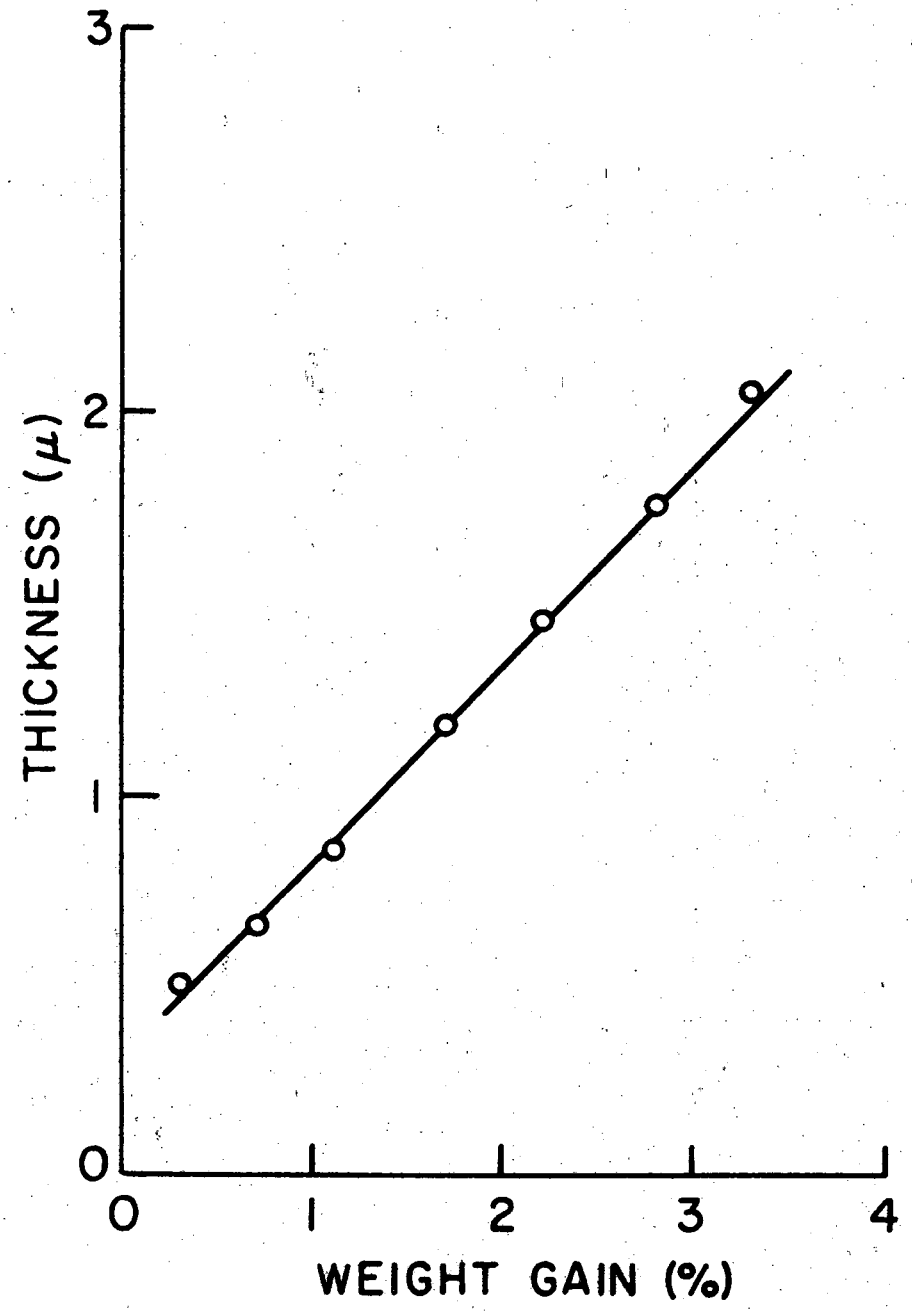

Fig. 5. Oxide thickness as a function of weight gain.

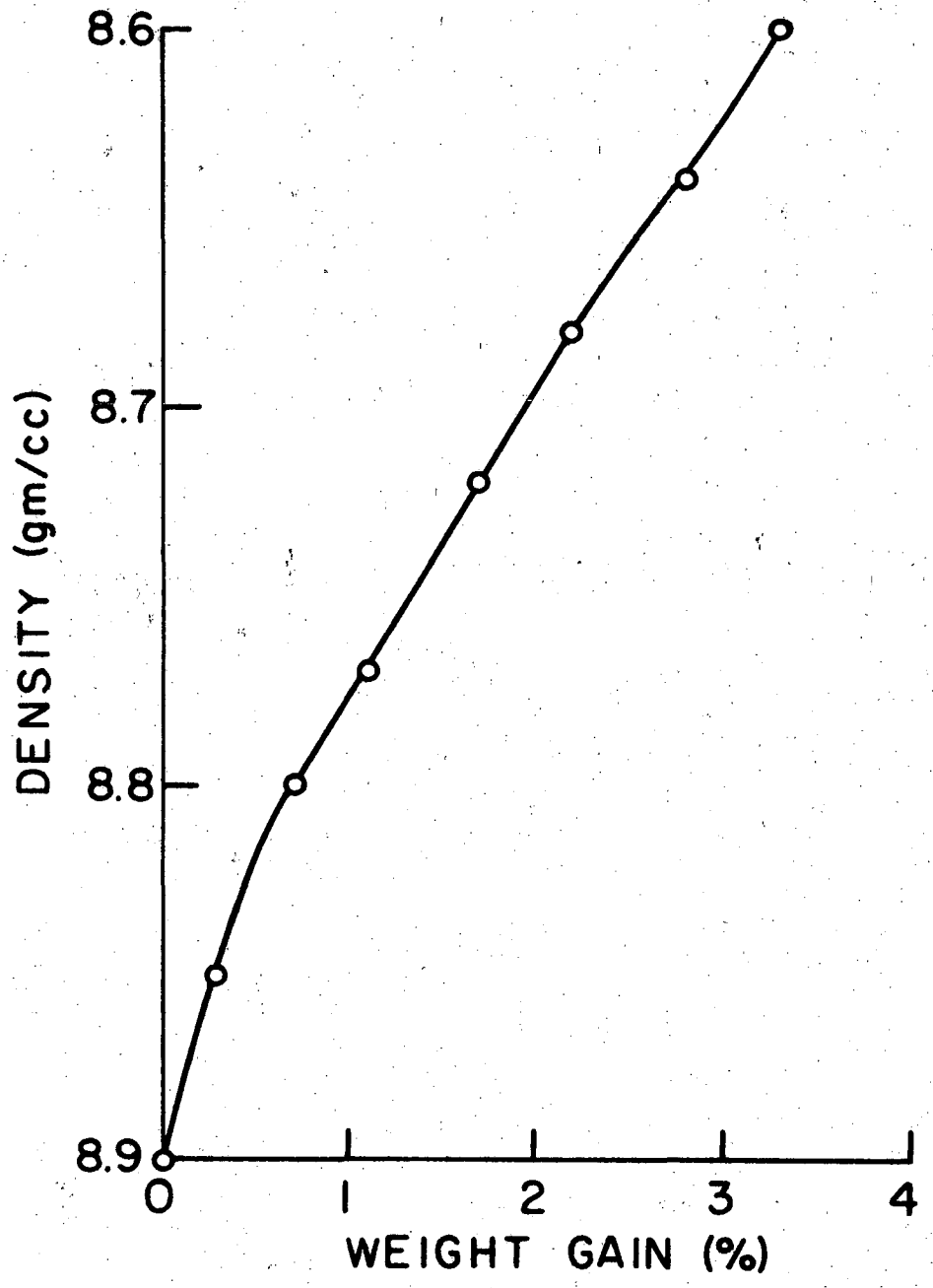

Fig. 6. Oxidized particle density as a function of weight gain.

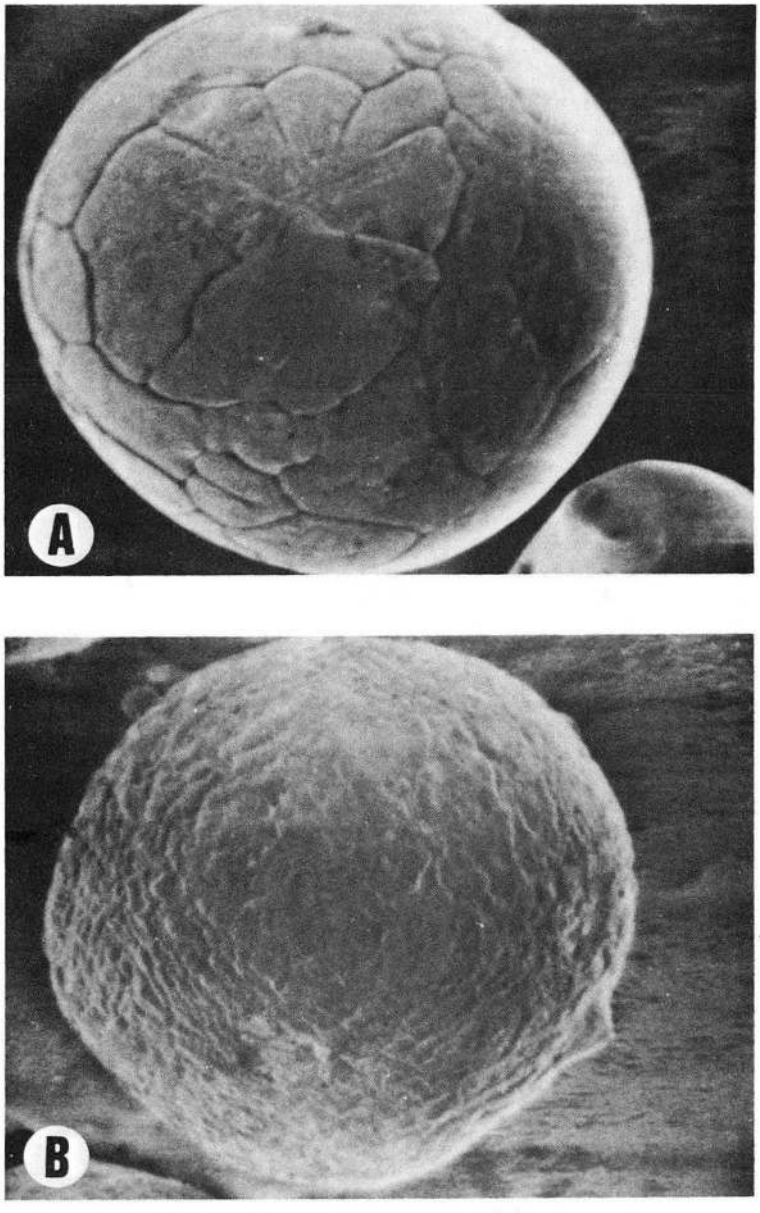

XBB 693-1887

Fig. 7

at 500 or 1000 psi for either 10 or 20 minutes at 700°C. The hot-pressing arrangement is shown in Fig. 8. Mixed powders were loaded into a graphite die and the die was positioned inside the vacuum chamber. A Pt-Pt 10% Rh thermocouple was inserted in the die body and the system was evacuated to less than a micron pressure. Resistance heating was employed using a 115 mil molybdenum heating coil. Rates of cooling from maximum temperature were controlled by the furnace's free cooling rate. A linear differential transformer attached to the bellows was used as a measure of the compaction of the sample in the die. The similar softening characteristics of the three glasses permitted the fabrication of theoretically dense composites at a single temperature.

Samples for the measurement of elastic properties were cut with a diamond saw from a 2 in. diameter x 1/4 in. thick vacuum hot-pressed glass disc. Strength measurements were made on .160 in. x .050 in. bars of various lengths that were cut from a 2 in. x .050 in. vacuum hot-pressed disc. The thin discs were cooled in an argon atmosphere to avoid cracking. An adequate flaw density was insured by abrading the tensile surface of the disc lightly with 240 grit SiC. Thermal expansion bars were also cut from the 2 in. diameter x 1/4 in. thick vacuum hot-pressed glass discs.

Uniaxial strengths were measured using a four-point loading device with a 3/4 in. overall span. Specimens were loaded with the abraded surface as the tensile surface. Several breakings were made with each specimen to obtain an average strength value. Resultant fracture surfaces were examined using a scanning electron microscope. Preparation included coating of the specimens with a 100-200Å layer of aluminum.

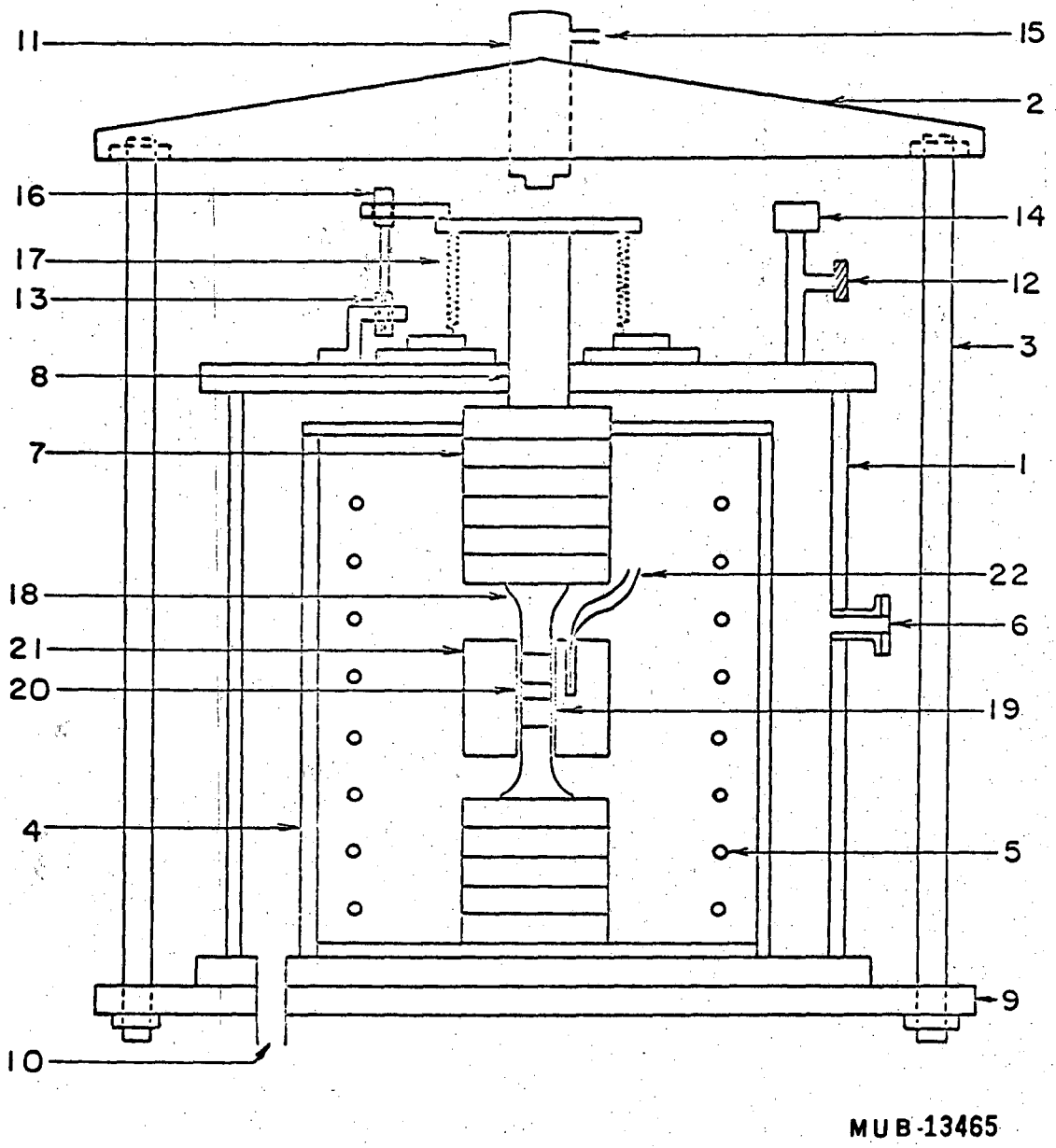

Fig. 8. Schematic diagram of hot press.

KEY

1. Vacuum cover
2. Top yoke
3. Load bearing column
4. Radiation shield
5. Mo heating coil
6. Sight window
7. Insulating spacers
8. Plunger
9. Bottom support plate
10. Vacuum port
11. Hydraulic ram
12. Air inlet
13. Linear variable differential transformer
14. Vacuum gauge
15. Pressure inlet
16. Micrometer head
17. Bellows
18. Graphite plunger
19. Graphite plug
20. Sample
21. Tungsten carbide die body
22. Thermocouple

Hot-pressed samples were sectioned and mounted in a clear casting resin. All samples were polished with a set of silicon carbide papers (240, 400, and 600 grit) and then finished on a series of diamond pastes (6, 2, and 1/2 micron diamond). Carbon was vapor deposited on the finished samples to provide a conductive surface suitable for electron microprobe analysis. The microprobe was used to examine the migration of the nickel oxide into the matrix glass.

IV. RESULTS AND DISCUSSION

A. D Glass System ($\alpha_G < \alpha_{Ni}$)

The system that was initially selected to investigate the effect of bonding on the strength of glass-metal composites was that used by Bertolotti and Fulrath.[10] Nickel microspheres that were pre-oxidized to varying degrees were used in conjunction with D glass in order to expand upon the anomalous strengthening observed for small particle sizes. It can be seen in Fig. 3 that a particle radius of 25μ and a volume fraction of 20% are sufficient to position the oxidized nickel-D glass system to the right of point A. The strength of the composite should, therefore, be a function of the mean free path in the matrix as calculated using Eq. (9). Either the residual or micromechanical stress concentrations may modify this calculated strength and would be reflected in the value of K in Eq. (10). Composites with a series of pre-oxidation treatments ranging from 0.18 to 5.8% weight gain were fabricated at 500 psi for 10 minutes at 700°C. Strengths of these samples are given in Table II and can be seen as a function of the amount of pre-oxidation in Fig. 9.

1. Non-bonded Composites

When there was a lack of bonding between the D glass and the nickel, the nickel shrank away from the D glass upon cooling from the fabrication temperature. This led to the formation of pseudoporosity and the resultant weakening of the composite. Since the two phases were not in contact, no internal stresses were introduced. The previously mentioned X-ray strain measurement technique was used to qualitatively determine the state of internal stress in this non-bonded D glass-nickel composite and provide a standard for comparison with other systems. Location of the

Table II

Crossbending strength and statistical data for oxidized nickel-D glass composites (10 min.)

Oxidation Temp(°C)	Oxidation Time (hrs.)	Weight Gain (%)	Average Strength (psi)	Number of Samples	Standard Deviation (% of average)
800	1/4	0.3	10,730	17	8.4
"	1/2	0.7	11,960	17	6.2
"	1	1.1	12,020	18	9.5
"	2	1.7	10,870	15	12.6
"	3	2.2	10,910	9	11.7
"	4	2.8	10,030	17	13.4
"	6	3.3	10,350	19	10.6
"	12 1/4	5.8	10,260	12	12.2
750	1/6	0.18	9,560	18	13.7
"	1/2	0.3	10,190	19	12.1
"	1 1/2	0.9	11,740	21	7.0
"	2	1.1	11,440	22	7.3
"	15	3.6	10,390	18	5.4
D glass alone			7,740	36	13.5
D glass & unoxidized Ni			6,440	32	8.1

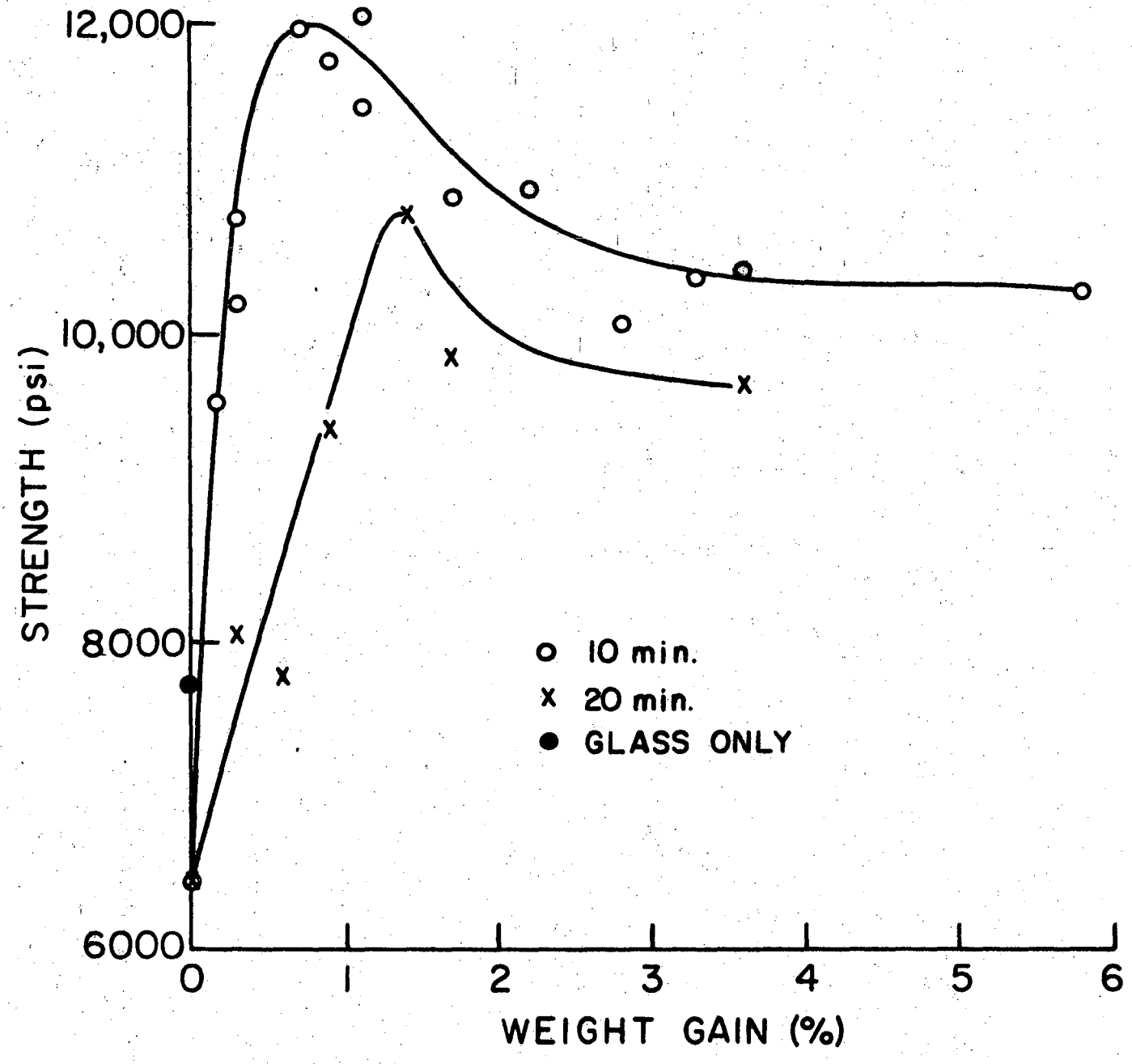

Fig. 9. Strength as a function of weight gain for the D glass-oxidized nickel series.

nickel (420) peak was taken as a gauge of the internal stress. It can be seen in Table III that the nickel (420) peak was located at 144.52° 2θ.

The hypothesis has been presented that the effect of micromechanical stress concentrations on the strength of a brittle material depends on the size of the Griffith flaw relative to the region over which the stress concentration acts. The effect of porosity on strength can be divided into two extremes.[9] In the first case the pore size is larger than the flaw size and the flaw lies entirely in material stressed to a high stress concentration and the introduction of even a single pore instantaneously decreases the strength of the nonporous material. The decrease in strength will correspond to the maximum stress concentration factor. In the second case the pore is considerably smaller than the Griffith flaw. The flaws will be unaffected by the stress concentrations near the pores. A decrease in strength as a function of the volume fraction of porosity should be observed, but without the precipitous decrease as in the first case. The Griffith flaw size generated by the standard specimen preparation technique used here can be obtained from point A in Fig. 3 and is found to be 150μ. By comparing this value with the 50μ diameter pseudoporosity formed in this case we would expect only a slight decrease in strength upon the addition of the first pore. The data confirm this expectation with a glass strength of 7,790 psi and a measured composite strength of 6,440 psi.

Fracture surfaces of the broken bars were examined using a scanning electron microscope and can be seen in Fig. 10. The path of fracture in a brittle material is altered by the inclusion of particles of a second phase or pores. If the inclusion is a pore, the fracture will propagate

TABLE III

Internal stress measurements

	2θ	d
D glass ($\alpha_G < \alpha_{Ni}$)		
No bond	144.52	0.80870
Bond	144.39	0.80900
S glass ($\alpha_G = \alpha_{Ni}$)		
No bond	144.51	0.80873
Bond	144.51	0.80873
M glass ($\alpha_G > \alpha_{Ni}$)		
No bond	144.54	0.80866
Bond	144.55	0.80863

to the pore and around its diameter, leaving a hemispherical cavity in the fracture surface. It can be seen in Fig. 10a that the fracture propagated directly to and around the sphere because of the tensile stress concentrations around a spherical cavity.

2. Bonded Composites

When a bond was created between the D glass and the nickel, the shrinkage of the nickel away from the glass upon cooling was prevented. The thermal contraction did, however, introduce a radial tensile stress which was evidenced in the X-ray strain measurements of Table 3 where the nickel (420) peak was shifted to 144.39° 2θ. This radial tensile internal stress was formed hydrostatically around the nickel sphere. It can be seen also from the strength data in Fig. 9 that the bond does, indeed, prevent the shrinkage of the nickel away from the glass and provide strengthening in a normally porous system.

The maximum stress concentration due to loading developed in this system was calculated using the following values and Eqs. (3-6):

G_G = 337 kbar (measured for D glass)

G_M = 724 kbar (measured for nickel)

μ_G = 0.2 (calculated for D glass)

μ_M = 0.4 (calculated for nickel)

$r = 25\mu = 9.84 \times 10^{-4}$ in

Maximum stress concentration will occur at the interface (R=r) and will be 1.348T for this system. Verification of the net radial tensile stress is seen in the scanning electron micrographs of the fracture surfaces (Fig. 10) showing fracture through the matrix and around the spheres rather than radially to the spheres. Had contact been maintained

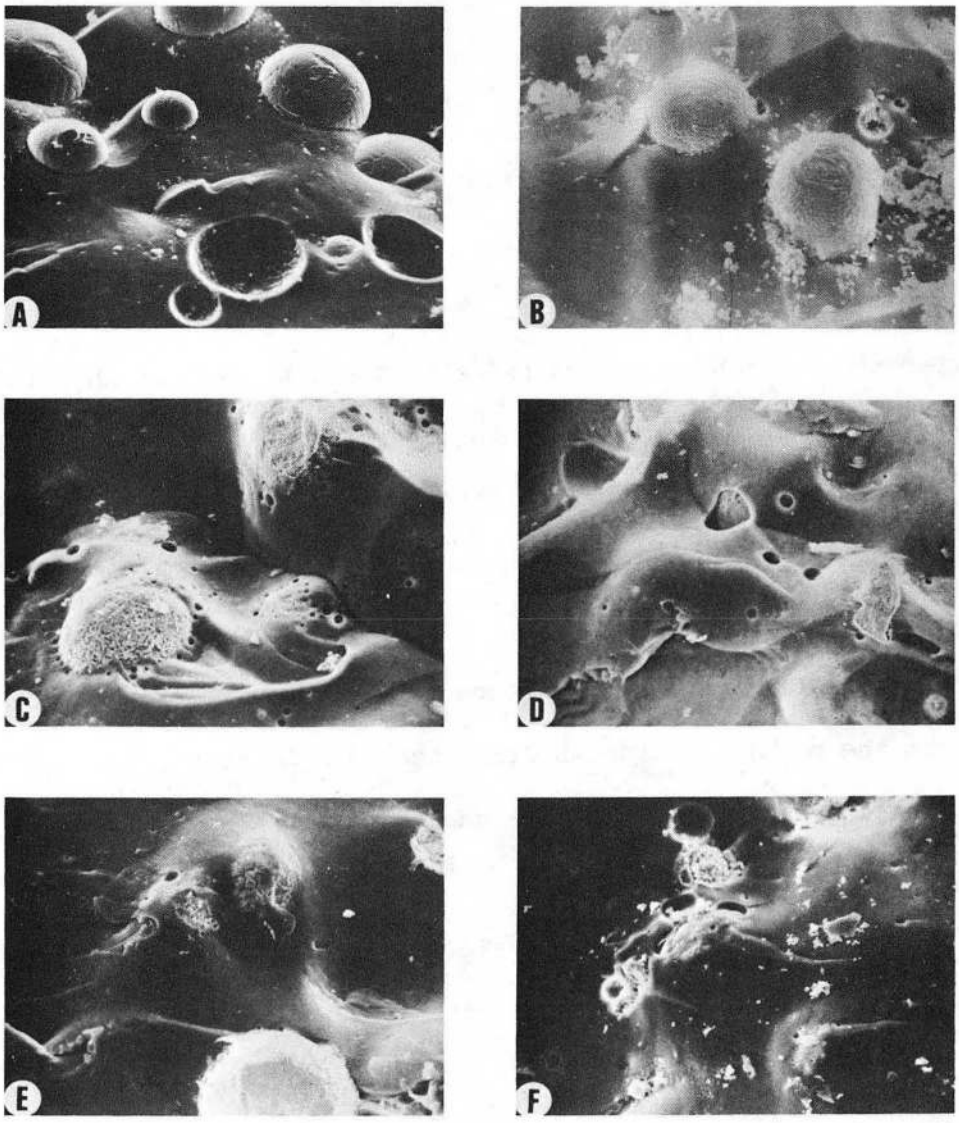

XBB 693-1889

Fig. 10

between the glass and the metal without the presence of a bond, this value of stress concentration would have been used in the strength calculation using Eq. (10).

The shape of the curve in Fig. 9 for the ten minute series corresponds to the bond hypothesis presented previously. An optimum bond (and also optimum strength) was observed. A pre-oxidation treatment of about 0.8% weight gain followed by the given hot-pressing treatment saturated the glass with nickel oxide at the sphere-glass interface. With lesser pre-oxidation treatments, the glass was less than saturated and a lower strength value was observed. With greater pre-oxidation treatments, a bulk oxide layer remained after saturation and the strength was correspondingly less. For a given pre-oxidation treatment, the greater length of time at temperature will allow more oxide to diffuse away from the particle, thus shifting the peak to greater weight gain. An increased pre-oxidation will be needed to yield the optimum amount of remaining oxide layer.

In order to test this hypothesis in the oxidized nickel-D glass system, a series of samples with varied pre-oxidation treatments was hot pressed at 700°C and 500 psi for 20 minutes. The data are presented in Table IV and the effect is clearly seen in Fig. 9. The optimum pre-oxidation was increased, but the reason for the decrease in the maximum strength is not clear.

A sample with 1.1% weight gain was examined using an electron beam microprobe in order to determine the extent of diffusion of the oxide into the glass. Nickel counts were taken from the center of a sphere radially outward into the glass matrix. It was found from three randomly

TABLE IV

Crossbending strength and statistical data for oxidized nickel-D glass composites (20 min.)

Oxidation Temp(°C)	Oxidation Time (hrs.)	Weight Gain (%)	Average Strength (psi)	Number of Samples	Standard Deviation (% of average)
750	1/2	0.3	8,030	18	7.3
"	1	0.6	7,780	13	15.9
"	1 1/2	0.9	9,390	14	15.2
"	3	1.4	10,750	18	10.7
"	4	1.7	9,830	18	10.6
"	15	3.6	9,670	16	9.9
D glass alone			7,740	36	13.5
D glass & unoxidized Ni			6,440	32	8.1

selected spheres that nickel was present to a distance of approximately 15μ from the sphere.

A calculation of the expected strength was made using Eq. (10). When contact is maintained between the glass and the nickel, the applied tensile load will tend to pull the glass away from the nickel and micromechanical stress concentrations will arise. The presence of a bond, however, tended to counter this separation and a simple strengthening due to a limitation of the flaw size was observed (K=1). Using the following values for the D glass-nickel system

$\theta = 0.2$

$R = 25\mu = 9.84 \times 10^{-4}$ in

$E = 11.7 \times 10^{6}$ psi (measured)

$\gamma = 10{,}000$ ergs/cm^2 = 0.0566 lb/in (assumed)

$K = 1$

Equation (10) gave an expected measured strength of 12,680 psi. This agrees well (5.2% error) with the maximum measured value of 12,020 psi in Table III. It therefore appears that the strength of a composite system is not determined by internal stresses but rather by the micromechanical stress concentrations developed on loading.

Representative fracture surfaces of bonded composites can be seen in Fig. 10. The path of fracture is altered when a chemical bond exists between the glass and the nickel. The fracture propagates through the glass around the inclusion, but still within the glass. This propagation through the matrix is most evident in the case of the optimum bond (Fig. 10d). Because of the thermal expansion variation among the saturated glass at the interface, the nickel, and the matrix glass, a radial internal

tensile stress is developed in the matrix. To relieve this tension, a fracture will propagate around the sphere at a finite distance in the glass phase.

B. S Glass System ($\alpha_G = \alpha_{Ni}$)

The next system to be investigated was one in which the thermal expansion of the glass was designed to equal that of the nickel. An attempt was made to design a glass whose thermal expansion coefficient was equal to that of nickel. The measured value of thermal expansion for S glass was 13.8 x 10^{-6} in/in °C which is very nearly the 13.9 x 10^{-6} in/in °C of nickel. In the following discussion they are considered close enough to be equal, but it should be recognized that the glass expansion is very slightly less than that of the nickel. In the S glass-nickel system it was necessary to change the particle size and volume fraction in order to remain in the flaw-limitation region. A particle size of 30μ and a volume fraction of 30 vol. % were selected in order to remain to the right of point B in Fig. 3. Once again a series of composites was hot pressed at 1000 psi for 10 minutes at 700°C with a wide range of pre-oxidation treatments. The data are given in Table V and can be seen in Fig. 11.

1. Non-bonded Composites

With matching expansions it would be expected that no internal stresses would be created upon cooling the composite from fabrication temperature. X-ray strain measurements in Table III show the nickel (420) peak to be found at 144.51° 2θ. By comparison with the non-bonded D glass standard of 144.52° 2θ there are essentially no internal stresses created

TABLE V

Crossbending strength and statistical data for oxidized nickel-S glass composites (30% spheres)

Oxidation Temp(°C)	Oxidation Time (hrs.)	Weight Gain (%)	Average Strength (psi)	Number of Samples	Standard Deviation (% of average)
750	1/6	0.18	10,690	14	5.6
750	1/2	0.3	11,410	15	5.2
750	1	0.6	12,460	11	6.4
800	1/2	0.7	10,790	16	9.0
750	1 1/2	0.9	11,540	13	3.5
750	2	1.1	11,090	13	5.3
750	4	1.7	11,000	17	9.2
800	3	2.2	10,690	11	8.1
750	10	2.8	10,570	17	8.6
800	6	3.3	9,870	13	6.8
750	15	3.6	9,850	13	8.1
S glass only			8,140	24	9.2
S glass & unoxidized Ni			10,380	9	8.2

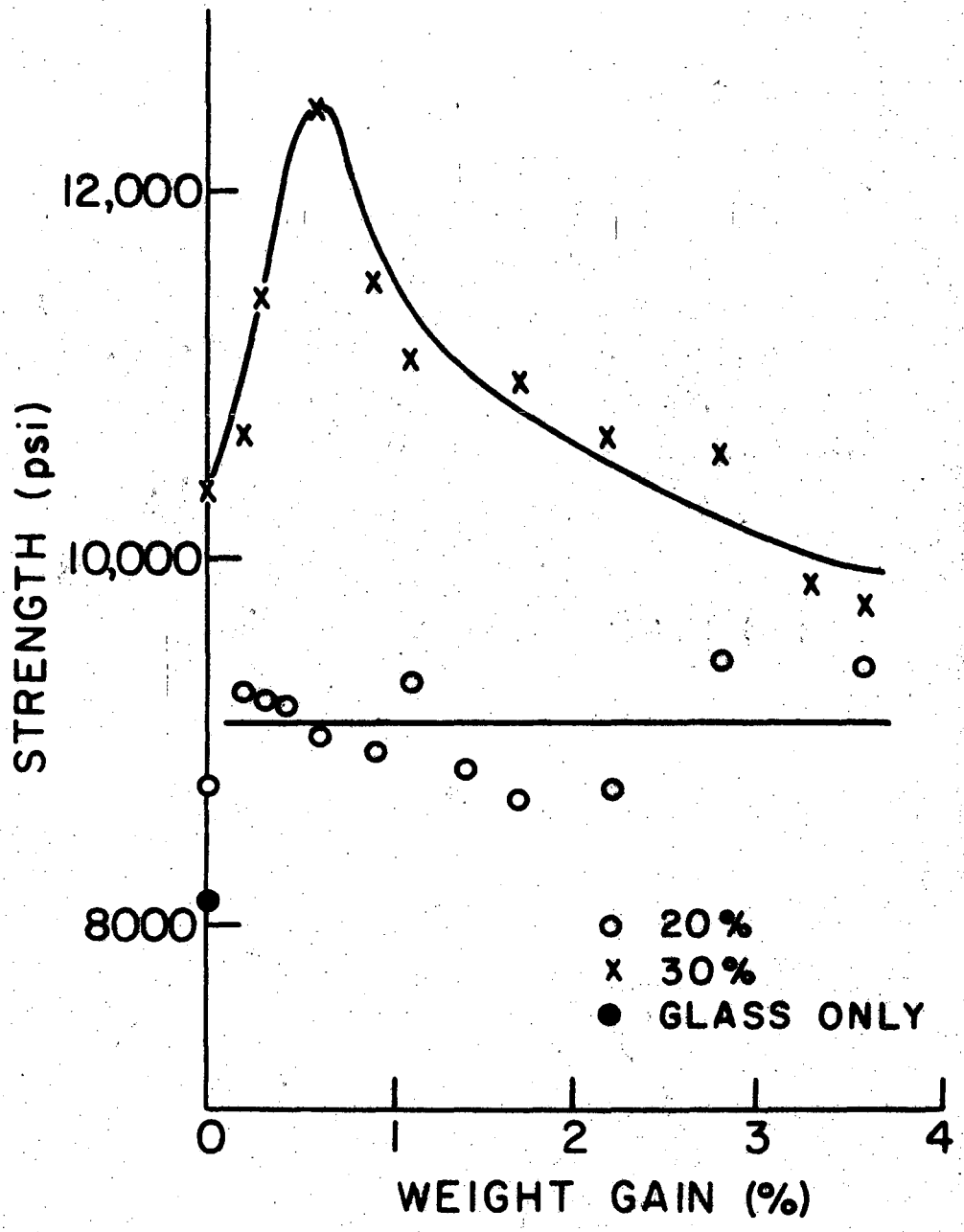

Fig. 11. Strength as a function of weight gain for the M glass-oxidized nickel series.

in fabrication.

Since contact is mechanically maintained between the glass and the metal upon cooling, stress concentrations are created on loading. A calculation of these stress concentrations was made using the following values and Eqs. (3-6):

G_G = 277 kbars (measured for S glass)

G_M = 724 kbars (measured for S glass)

μ_G = 0.2 (calculated for S glass)

μ_M = 0.4 (calculated for S glass)

$r = 30\mu = 11.8 \times 10^{-4}$ in.

For an applied load of T, the maximum stress concentration as shown in Fig. 1 is 1.374T. Once again the maximum stress concentration would be expected to occur at the interface (R=r). This concentration of stress means that, for an applied load of T, there will be an area (shown in Fig. 1) within the composite where a stress of 1.374T was developed.

The expected strength was calculated using Eq. (10) and recalling that stress concentrations existed as a result of the maintenance of contact between sphere and glass upon cooling from the fabrication temperature. Using the stress concentration factor of 1.374T and a measured Young's modulus of 9.8×10^6 psi, a value of 10,110 psi was calculated for the non-bonded composite. This compares well (2.7% error) with the average measured value of 10,380 psi that was found for the nine bars that were broken.

Scanning electron micrographs of the fracture surfaces of the broken bars can be seen in Fig. 12. In the absence of a bond it can be seen (Fig. 12a) that the fracture propagated to the sphere and around it at

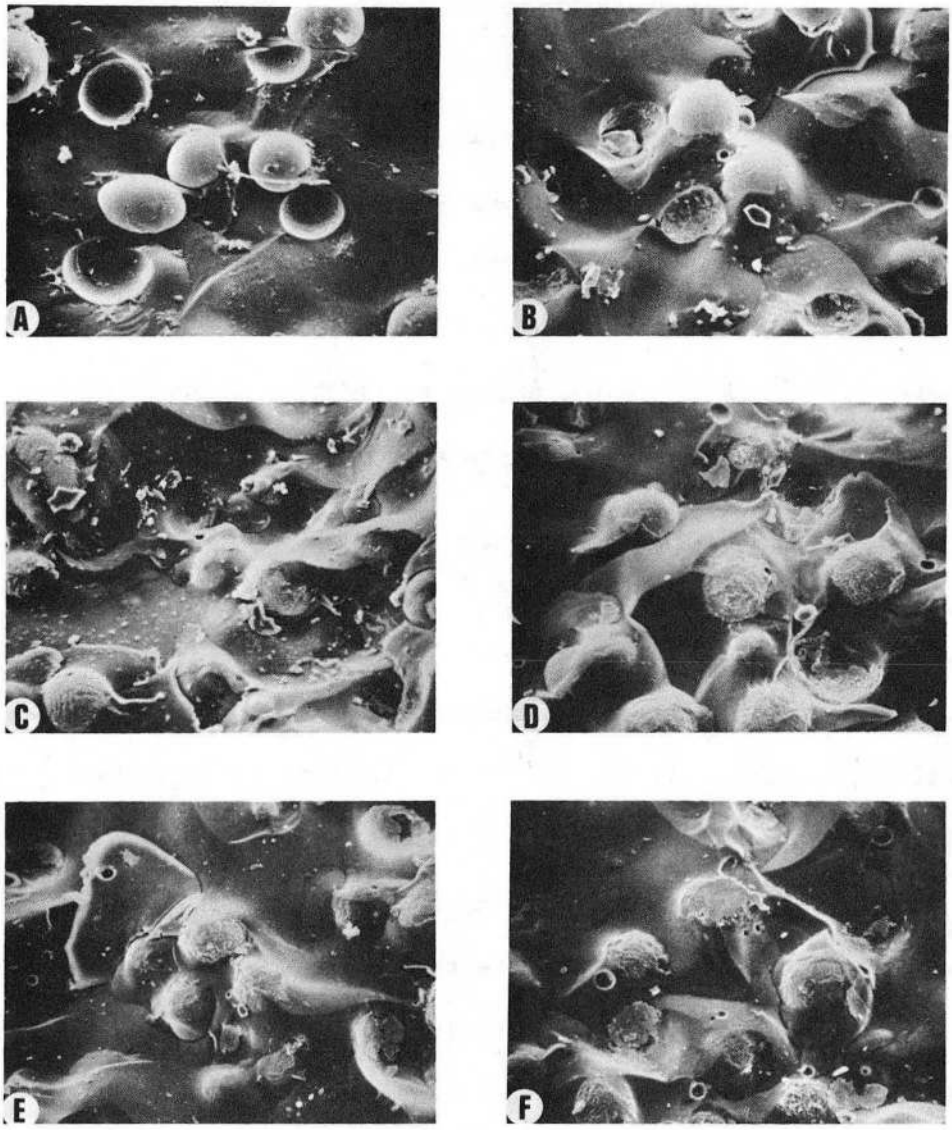

XBB 693-1886

Fig. 12

the sphere-glass interface. Hemispherical cavities remain as evidence of spheres in the opposite fracture surface.

2. Bonded Composites

In the D glass sytem the bond played an important role in that it prevented the shrinkage of the nickel away from the glass. With matching thermal expansions, however, this role is unnecessary and the bond had no effect upon internal stresses. This is evidenced by the X-ray strain measurements of Table III which showed no shift of the nickel (420) peak with the formation of a bond. The same location, 144.51° 2θ, was observed as for the non-bonded case.

The shape of the curve for the 30 vol % series in Fig. 11 once again shows an optimum pre-oxidation treatment in order to obtain the optimum bond and therefore the maximum strength for the given fabrication process. With lesser pre-oxidation treatments we once again see a lower strength because saturation was not reached. With greater pre-oxidation treatments, a bulk oxide layer remained after saturation and a lower strength is observed. In order to illustrate the necessity of controlling the average mean free path between particles, a series to the left of point B in Fig. 3 with only 20 vol. % of 25μ diameter spheres was hot pressed. In this instance the flaw-limitation mechanism is not applicable and we would expect to see little effective strengthening upon the addition of the second phase. The results of this series are given in Table VI and can be seen in Fig. 11.

The expected strength of a bonded S glass-nickel composite was calculated using Eq. (10). Once again it was observed that the presence of a bond counteracted the concentration of stress developed during loading.

TABLE VI

Crossbending strength and statistical data for oxidized nickel-S glass composites (20% spheres)

Oxidation Temp (°C)	Oxidation Time (hrs.)	Weight Gain (%)	Average Strength (psi)	Number of Samples	Standard Deviation (% of average)
750	1/6	0.18	9,280	13	4.7
750	1/2	0.3	9,230	17	9.8
750	1	0.6	9,040	12	13.6
750	1 1/2	0.9	8,940	11	4.8
750	2	1.1	9,320	20	9.0
750	3	1.4	8,860	15	6.8
750	4	1.7	8,690	16	9.6
800	3	2.2	8,740	16	14.1
750	10	2.8	9,460	19	10.9
750	15	3.6	9,410	19	7.9
S glass only			8,140	24	9.2
S glass & unoxidized Ni			8,770	18	6.0

Using

$\phi = 0.3$

$R = 30\mu = 11.8 \times 10^{-4}$ in

$E = 9.8 \times 10^{6}$ psi

$K = 1$

the strength to be expected was calculated as 13,900 psi. The maximum measured value in Table V is 12,460 psi and this is 10.3% lower than anticipated.

It is evident, as in the D glass system, that the proper amount of pre-oxidation in order to obtain the maximum strength is critical. Just slightly more or less than the optimum pre-oxidation will yield a much weaker composite.

Characteristic fracture surfaces of the 30 vol. % bonded composites are seen in Fig. 12. Once again a small radial tension is developed as a result of the slight thermal expansion variation among the saturated glass, the nickel, and the matrix glass. The bond is evident in Fig. 12b-d by observing glass adhering to the nickel spheres in the fracgure surface. Its magnitude can be compared with the bonded D glass-nickel system shown in Fig. 10.

A sample with 0.9% weight gain was examined with the electron beam microprobe. Nickel counts were taken as the beam traversed radially from the center of a sphere outward into the matrix. Three randomly selected spheres yielded a distance of 13μ from the sphere at which nickel was detected.

C. M Glass System ($\alpha_G > \alpha_{Ni}$)

The third system to be investigated was one in which the thermal

expansion of the glass is greater than that of the nickel. In this case the interface between the glass and the second phase is formed mechanically by the contraction of the glass around the sphere during cooling. In addition, a chemical bond was introduced by the pre-oxidation process. Once again a change in the volume fraction of 35 vol. % of 30μ spheres was dictated in order to preserve the flaw-limitation mechanism (Fig. 3) and remain to the right of point C. A series of composites was hot pressed at 1000 psi for 10 minutes at 700°C with a range of pre-oxidation treatments. The strength values are given in Table VII and can be seen in Fig. 13.

1. Non-bonded Composites

With the thermal expansion coefficient of the glass greater than that of the nickel, the glass contracted around the nickel microspheres upon cooling from the fabrication temperature. This contraction around the nickel was sufficient to put the nickel into a slight compression as is evidenced by the X-ray strain measurements in Table III. The nickel (420) peak was detected at 144.54° 2θ compared with 144.52° 2θ for the non-bonded D glass standard.

Only mechanical contact is maintained between the glass and the nickel in the non-bonded composite. Under the applied tension the tendency of the glass to pull away from the nickel gave rise to a micro-mechanical stress concentration. The maximum stress concentration in this system was calculated using the following values and Eqs. (3-6).

G_G = 290 kbars (measured for M glass)

μ_G = 0.2 (calculated for M glass)

$r = 30\mu = 11.8 \times 10^{-4}$ in

$\phi = 0.35$

TABLE VII

Crossbending strength and statistical data for oxidized nickel-M glass composites (10 min.)

Oxidation Temp (°C)	Oxidation Time (hrs.)	Weight Gain (%)	Average Strength (psi)	Number of Samples	Standard Deviation (% of average)
750	1/6	0.18	13,630	20	9.4
750	1/2	0.3	14,240	16	6.1
750	1	0.6	15,260	19	6.1
800	1/2	0.7	14,580	7	8.8
750	1 1/2	0.9	15,000	17	10.9
750	2	1.1	14,800	11	5.3
750	4	1.7	15,390	14	5.2
800	3	2.2	15,120	9	7.3
750	15	3.6	15,320	10	6.9
M glass only			9,920	13	6.1
M glass & unoxidized Ni			11,860	12	7.0

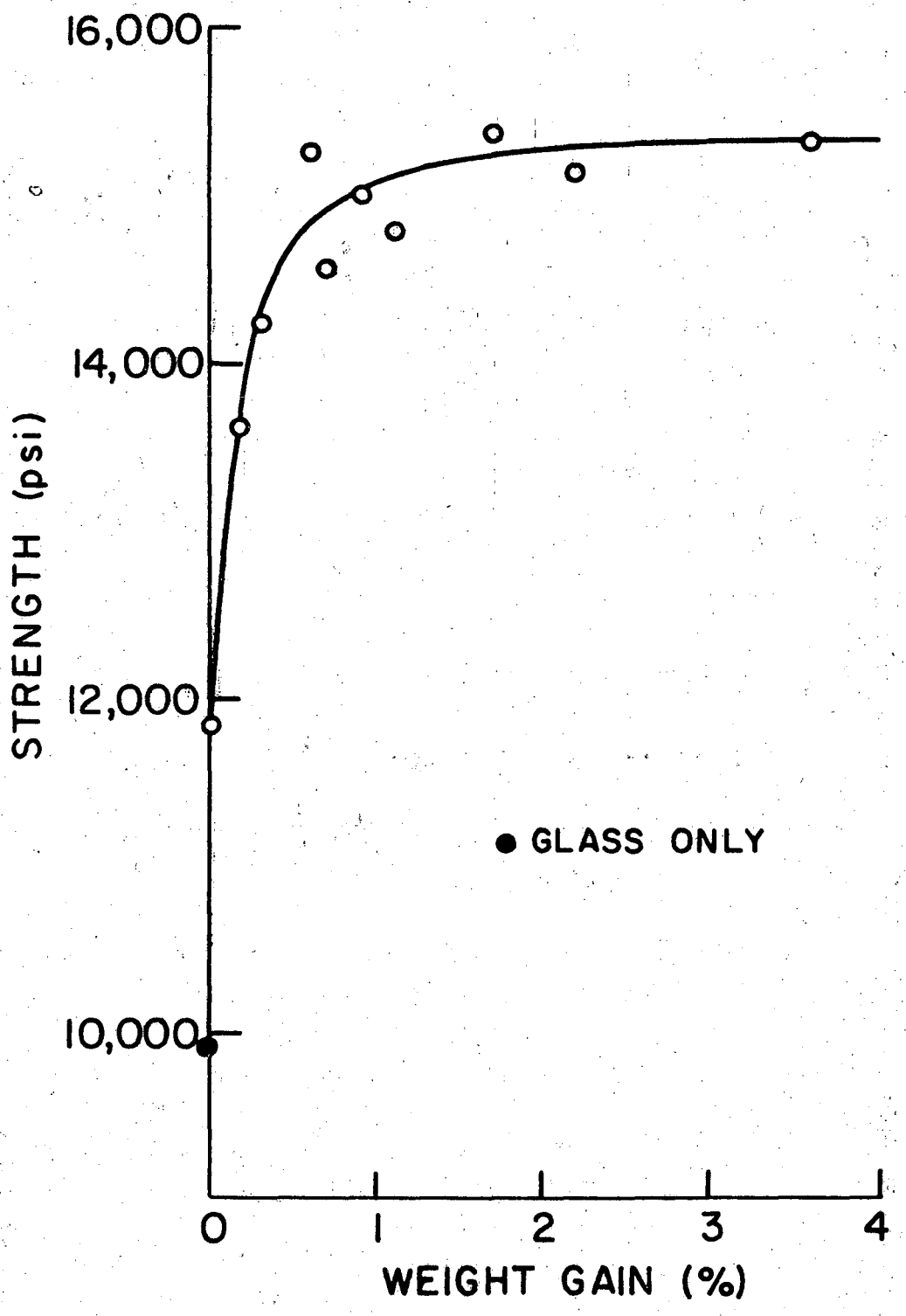

Fig. 13. Strength as a function of weight gain for the M glass-oxidized nickel series.

When a load of T is applied to the composite, a stress concentration of 1.366T was formed at the glass-nickel interface as shown in Fig. 1.

Equation (10) was used to calculate the strength to be expected from the non-bonded composite. Using the calculated stress concentration factor and a measured value of 10.2×10^6 psi for the Young's modulus, a strength of 11,610 psi was predicted. This agrees very well (2.1% error) with the actual measured value of 11,860 psi for the twelve bars broken.

Fracture surfaces of the broken bars in the M glass-nickel system were examined with the scanning electron microscope. The fracture path in the non-bonded case can be seen in Fig. 14a. Once again the fracture propagates toward the nickel and around it, leaving a hemispherical cavity in the fracture surface. This would be expected because it relieves the biaxial tension resulting from the internal stress.

2. Bonded Composites

As in the case of the matching thermal expansion system, the existence of a bond did not affect the internal stresses. This was illustrated by the X-ray strain measurements which located the nickel (420) peak at 144.55° 2θ for the bonded composite compared with 144.54° 2θ for the non-bonded composite.

The presence of a bond greatly enhanced the strength of composites in this system. As can be seen in Fig. 13, strengthening was limited until a pre-oxidation treatment was used which would saturate the glass under the hot-pressing conditions. A sample made with spheres pre-oxidized to 0.9% weight gain was examined with the electron microprobe. Nickel was detected to a distance of 18μ from the glass-nickel interface.

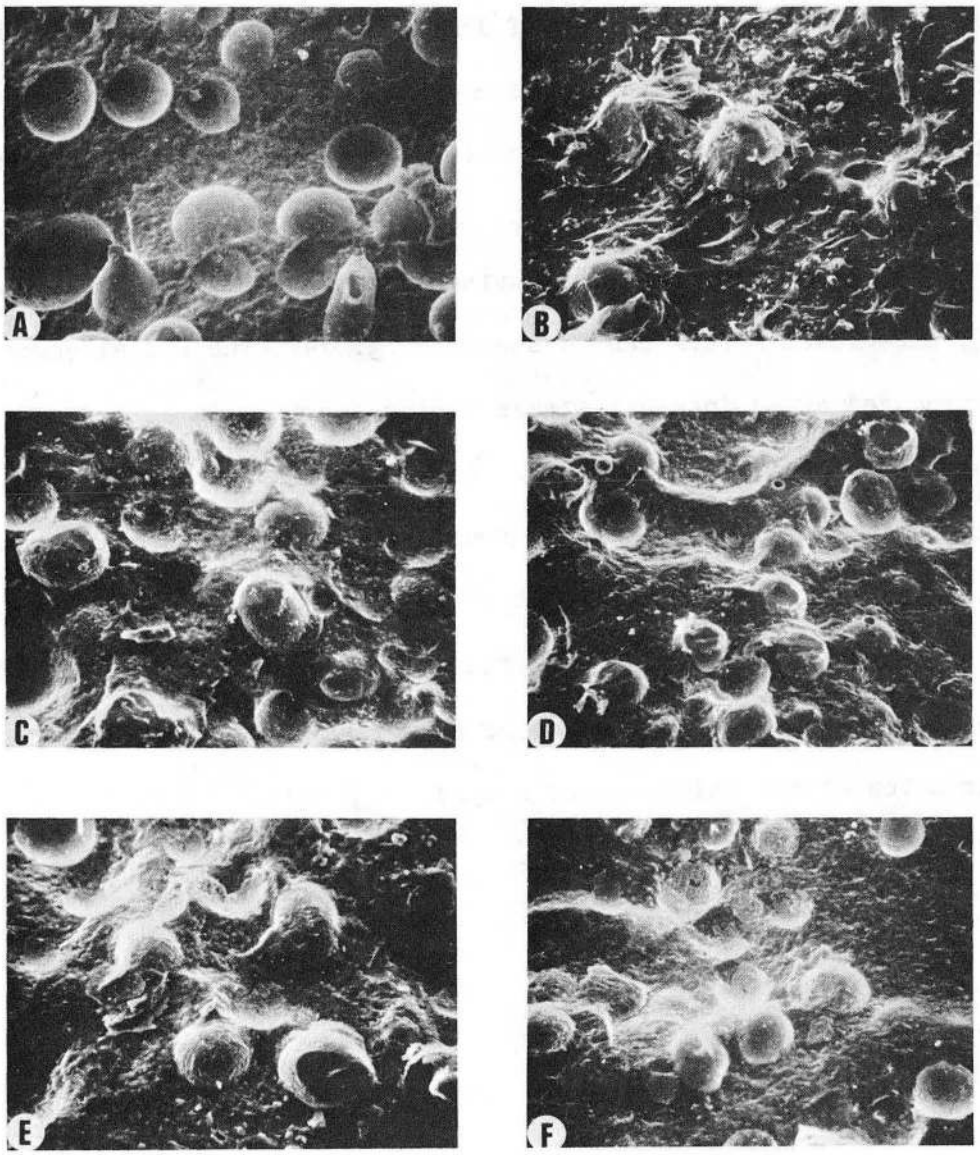

XBB 693-1888

Fig. 14

Existence of the bond again prevented the glass from pulling away from the nickel under an applied tensile load (K=1). Equation (10) yielded a predicted strength of 15,880 psi for the bonded composite. A comparison of this value with the maximum strength measured in Table VII of 15,390 psi again shows a good (3.1% error) agreement for the 14 samples broken.

Representative fracture surfaces of the bonded composites in the M glass-nickel system can be seen in Fig. 14. The radial compression introduced as an internal stress during fabrication correspondingly set up a tangential tensile stress. In order to attempt to relieve this tangential tensile stress, the fracture proceeded directly to the nickel microspheres and around them at the glass-nickel interface in spite of the presence of the bond. Careful examination of the pictures shows (as in Fig. 14e) some adhesion of the glass to the microspheres in confirmation of the existence of a bond.

V. SUMMARY

Composites were hot pressed using glasses of varying thermal expansion coefficient and nickel with varying degrees of pre-oxidation in order to study the effect of chemical bonding between the nickel and glass upon strength and fracture behavior. Glasses with a thermal expansion coefficient lower than, higher than, and matching that of nickel were compounded. The bond was developed by the migration of oxide at the fabrication temperature and the resultant saturation of the glass with the oxide in the vicinity of the nickel.

When no bond was present, a lower expansion glass led to pseudoporosity with the resultant weakening and a higher expansion glass led to strengthening due to mechanical contraction of the glass around the nickel upon cooling. No matter what the relative thermal expansions were, micromechanical stress concentrations were developed upon loading. Strengthening was observed with both matching and higher thermal expansion glasses, but the micromechanical stress concentrations reduced the strength far below that expected from a simple Griffith flaw limitation mechanism.

The presence of the optimum bond between phases dramatically increased the strength of the composites. In the case of the low expansion glass the bond prevented the formation of pseudoporosity by halting shrinkage of the nickel away from the glass. In all cases the existence of a bond between phases counteracted the micromechanical stress concentration developed upon loading. The strength was then regulated by a simple Griffith flaw limitation mechanism.

Internal stresses that are developed within the composite during cooling from the fabrication temperature control the path of fracture.

Differences in thermal expansion near the nickel can create either radial or tangential tension in the matrix. In order to relieve tangential tension, such as that developed in the bonded, high expansion matrix system, the fracture propagates directly to the nickel sphere. In order to relieve radial tension, such as that developed in the bonded, low expansion matrix system, the fracture propagates around the nickel, but still within the glass matrix.

The strength and path of fracture were found to be independent. Internal stresses control the path of fracture, macromechanical stress concentrations control the strength, and the bond counteracts the micromechanical stress concentrations to produce an even greater strength.

ACKNOWLEDGMENT

The scanning electron microscope used was operated within the Electronics Research Laboratory, University of California. It was purchased under Grant No. GB-6428 from the National Science Foundation and is operated under Grant No. GM15536 from the National Institute of Health.

The writer is greatly indebted to Professor R. M. Fulrath under whose guidance the present investigation was conducted. Thanks are extended to Mike Nemanic for assistance with the scanning electron microscope and to George Dahl for help in specimen preparation.

This work was done under the auspices of the United States Atomic Energy Commission.

REFERENCES

1. R. M. Fulrath, "Internal Stresses in Model Ceramic Systems," J. Am. Ceram. Soc., 42 (9) 423-429 (1959).

2. L. A. Jacobson, "Strength of a Two-Phase Model System" (M.S. Thesis) University of California, Berkeley, 1959.

3. D. O. Nason, "Effect of Interfacial Bonding on Strength of a Model Two-Phase System" (M.S. Thesis), University of California, Berkeley, 1962.

4. P. L. Studt and R. M. Fulrath, "Mechanical Properties and Chemical Reactivity in Mullite-Glass Systems," J. Am. Ceram. Soc., 45(4) 182-188 (1962).

5. D. P. H. Hasselman and R. M. Fulrath, "Effect of Alumina Dispersions on Young's Modulus of a Glass," J. Am. Ceram. Soc. 48(4) 218-219 (1965).

6. D. P. H. Hasselman and R. M. Fulrath, "Effect of Spherical Tungsten Dispersions on Young's Modulus of a Glass," J. Am. Ceram. Soc., 48(10) 548-549 (1965).

7. D. P. H. Hasselman and R. M. Fulrath, "Proposed Fracture Theory of a Dispersion-Strengthened Glass Matrix," J. Am. Ceram. Soc., 49(2) 68-72 (1966).

8. G. Einmahl, "Strength in a Two-Phase Model System with Fiber Reinforcement" (M.S. Thesis), University of California, Berkeley, 1966.

9. D. P. H. Hasselman and R. M. Fulrath, "Micromechanical Stress Concentrations in Two-Phase Brittle Matrix Ceramic Composites," J. Am. Ceram. Soc., 50(8) 399-404 (1967).

10. R. L. Bertolotti and R. M. Fulrath, "Effect of Micromechanical Stress Concentrations on Strength of Porous Glass," J. Am. Ceram. Soc. 50(11) 558-562 (1967).

11. M. A. Stett and R. M. Fulrath, "Chemical Reaction in a Hot-Pressed Al_2O_3-Glass Composite," J. Am. Ceram. Soc. 50 (12) 673-676 (1967).

12. M. A. Stett and R. M. Fulrath, "Strengthening by Chemical Bonding in a Brittle Matrix Composite," J. Am. Ceram. Soc., 51 (10) 599-600 (1968).

13. Y. Nivas, "Limitation of Griffith Flaws in Glass-Matrix Composites" (M.S. Thesis), University of California, Berkeley, 1968.

14. Jorgen Selsing, "Internal Stresses in Ceramics," J. Am. Ceram. Soc. 44 (8) 419 (1961).

15. L. N. Grossman and R. M. Fulrath, "X-ray Strain Measurement Techniques for Ceramic Bodies," J. Am. Ceram. Soc., 44 (11) 567-71 (1961).

16. J. N. Goodier, "Concentration of Stress Around Spherical and Cylindrical Inclusions and Flaws," J. Appl. Mech., 1 (1) 39-44 (1933).

17. J. A. Pask and R. M. Fulrath, "Fundamentals of Glass-to-Metal Bonding: VIII," J. Am. Ceram. Soc., 45 (12) 592-96 (1962).

18. R. L. Fullman, "Measurement of Particle Sizes in Opaque Bodies," Trans. AIME, 197 (3) 447-52 (1953).

19. S. Spinner and W. E. Tefft, "Method for Determining Mechanical Resonance Frequencies and for Calculating Elastic Moduli from these Frequencies," Am. Soc. Testing Mater. Proc., 61, 1221-38 (1961); Ceram. Abstr. 1962, October, p. 248g.

20. G. Pickett, "Equations for Computing Elastic Constants from Flexural and Torsional Resonant Frequencies of Vibrations of Prisms and Cylinders," Am. Soc. Testing Mater. Proc., 45, 846 (1945).

21. D. P. H. Hasselman, "Tables for Computation of Shear Modulus and Young's Modulus of Elasticity from Resonant Frequencies of Rectangular Prisms," The Carborundum Company, Niagara Falls, New York, 1962.

TECHNICAL INFORMATION DIVISION
LAWRENCE RADIATION LABORATORY
UNIVERSITY OF CALIFORNIA
BERKELEY, CALIFORNIA 94720